JACS
JOURNAL OF THE AMERICAN CHEMICAL SOCIETY
Article
pubs.acs.org/JACS

Ammonia Binds to the Dangler Manganese of the Photosystem II Oxygen-Evolving Complex

Paul H. Oyala,[†] Troy A. Stich,[†] Richard J. Debus,[‡] and R. David Britt*,[†]

[†]Department of Chemistry, University of California, Davis, Davis, California 95616, United States
[‡]Department of Biochemistry, University of California, Riverside, Riverside, California 92521, United States

Supporting Information

ABSTRACT: High-resolution X-ray structures of photosystem II reveal several potential substrate binding sites at the water-oxidizing/oxygen-evolving 4MnCa cluster. Aspartate-61 of the D1 protein hydrogen bonds with one such water (W1), which is bound to the dangler Mn4A of the oxygen-evolving complex. Comparison of pulse EPR spectra of $^{14}NH_3$ and $^{15}NH_3$ bound to wild-type *Synechocystis* PSII and a D1-D61A mutant lacking this hydrogen-bonding interaction demonstrates that ammonia binds as a terminal NH_3 at this dangler Mn4A site and not as a partially deprotonated bridge between two metal centers. The implications of this finding on identifying the binding sites of the substrate and the subsequent mechanism of dioxygen formation are discussed.

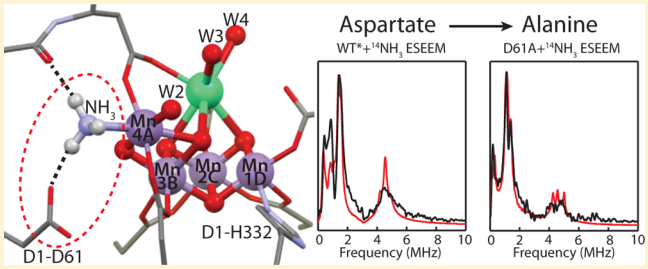

INTRODUCTION

The oxygen-evolving complex (OEC) of the photosystem II (PSII) reaction center oxidizes two substrate water molecules to form O_2 and bioactivated electrons and protons. The four-electron oxidation of these two substrate waters begins with photon-driven electron transfer at a chlorophyll moiety (P_{680}) coupled via a transient $Y_Z^{\bullet}$ tyrosine radical (at D1-Y161) to Mn cluster oxidation in a series of "S-state" intermediates S_0−S_4,[1] with O_2 released in the $S_4 \rightarrow S_0 + O_2$ transition on the millisecond time scale. Recent high-resolution X-ray structures of PSII[2,3] provide a detailed picture of the OEC poised primarily in the dark-stable S_1-state of the S-state cycle (Figure 1A). The OEC contains four high-valence manganese ions. Three of these, Mn1D, Mn2C, and Mn3B, join with a single Ca^{2+} to form a mixed metal Mn_3Ca-oxo core, as demonstrated earlier by Ferreira et al.[4] in a lower resolution X-ray structure. In the S_1-state structure the fourth Mn4A is linked to this 3Mn-Ca-oxo core via a pair of oxo bridges (O4 and O5). This Mn4A is often referred to as the "dangler Mn" based on an early EPR/ENDOR/EXAFS-based model of the OEC predating PSII X-ray structures[5] [electron paramagnetic resonance (EPR); electron nuclear double resonance (ENDOR); extended X-ray absorption fine structure (EXAFS)].

Even with the current high-resolution structure, there is ambiguity as to which of several waters or water-derived ligands in the OEC correspond to the two substrate waters that are oxidized to make O_2. This is an unusual aspect to this enzyme, as the substrate is also the solvent. In the S_1-state there are two terminal water ligands, W1 and W2, bound to the dangler Mn4A. An additional two waters, W3 and W4, are bound to the Ca^{2+} ion of the core. There are several oxo bridges internal to the OEC that could in principle also serve as sources of oxygen. And there are several nearby waters observed in the X-ray structure (not shown in Figure 1) which could potentially bind to Mn subsequent to the S_1-state, which is currently the only state resolved at the atomic level.

In terms of the mechanism of O−O bond formation, most attention has focused on two specific models, each of which comes with specific assignments for the two substrate waters. At the S_3 state, all four of the Mn ions are in the Mn(IV) oxidation state.[6] Unless the O−O bond is formed directly from S_3 and the $Y_Z^{\bullet}$ tyrosine radical,[7] a branch point occurs upon further oxidation to a true S_4-state intermediate,[8] with the two limiting electronic structure options of: (a) oxidation of Mn(IV) to Mn(V) or (b) oxidation of a Mn ligand, possibly substrate, to form a ligand radical.

Option (a): a Mn(V)═O intermediate. This is an interesting option, because in biology, outside of PSII, the use of Mn(IV) is rare,[9] and there are no known examples of Mn(V)-containing intermediates. Well before the modern OEC X-ray structures, it was recognized that the presence of high-valence Mn in close proximity to Ca^{2+} in the OEC provides a possible O−O bond forming route, specifically via a nucleophilic attack by a Ca-bound water or hydroxide on an electron-deficient Mn species such as Mn(V)═O.[10−12] In the context of the current X-ray structure (Figure 1), a geometrical basis of such an O−O bond forming reaction is quite evident, with the dangler Mn4A serving as the electrophile, perhaps as a Mn(V)═O species at the S_4-state, in close proximity to Ca^{2+}-bound water. In this mechanism the crystallographically defined waters W2 and W3 are prime candidates for the substrate waters.[13] Moreover, there

Received: May 7, 2015
Published: June 17, 2015

ACS Publications © 2015 American Chemical Society

DOI: 10.1021/jacs.5b04768
J. Am. Chem. Soc. 2015, 137, 8829−8837

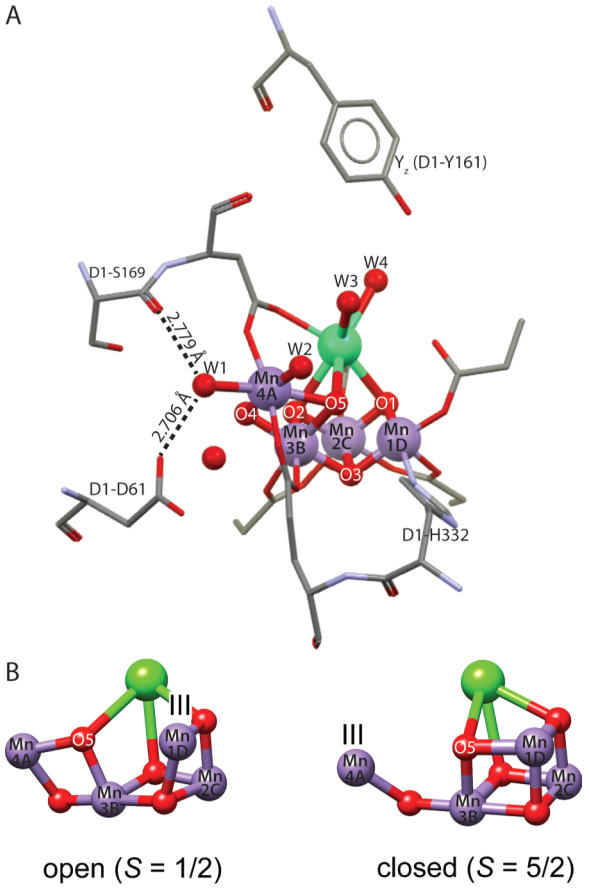

Figure 1. (A) X-ray structure of the OEC poised in the S_1-state (PDB ID 4UB6).[3] Colors: purple, Mn; green, Ca; and red, O. (B) Proposed core OEC structures of "open" and "closed" conformations of the S_2-state,[18] including the location of the unique Mn(III) ion.

is recent synthetic precedence for generating high-spin (S = 1) Mn(V)═O complexes as central to this mechanism.[14−16]

Option (b) a radical intermediate. The most-cited mechanism for O−O bond formation invoking such a radical intermediate is that proposed by Siegbahn,[17] which centers upon the unique bridging oxygen denoted O5 (Figure 1A) . DFT calculations based on the X-ray structure reveal a conformational flexibility in the S_2-state hinging upon this O5 bridge.[18] In an "open" S_2-state form similar to the S_1-state structure, O5 is ligated to Mn4A, and this geometry is modeled to give rise to the S = 1/2 multiline EPR signal, whereas in the "closed" form O5 shifts to bind to Mn1D, creating a Mn_3O_4Ca cubane plus dangler Mn configuration that produces the S = 5/2, g = 4.1 S_2-state EPR signal (Figure 1B).[18] These two conformations are calculated to be close enough in energy to allow small chemical or physical perturbations to shift the OEC geometry between forms and their associated spectroscopic signals, and the proposed interconversion between the open and closed forms provides a mechanism for the O5 μ-oxo bridge to exchange faster than μ-oxo bridges of simple high-valence Mn dinuclear complexes, which are quite inert to oxygen exchange.[19] Siegbahn[20] provides a detailed discussion of these points from a computational perspective. In the context of this flexible S_2-state model, the transition to the S_3-state is modeled with the binding of a new water-derived substrate to Mn, specifically as a hydroxyl ligand to Mn1D (which is 5-coordinate in the open model for S_2).[6,17] The O−O bond then forms via a radical coupling between the new Mn1D-bound OH and the proximal O5 bridge.[6,17]

Thus, the two most cited mechanisms for forming O_2 propose two different pairs of substrate molecules: W2 and W3 versus O5 and an S_3-bound OH^-. Therefore, it is crucial to pursue approaches that can identify which of the many potential substrate sites in the OEC can be actual substrates or, alternatively, to eliminate one or more potential candidates. One approach along these lines is to probe the OEC coordination by substrate analogs and inhibitors which can be spectroscopically distinguished from water, for example, with additional specific nuclear isotopes such as ^{13}C, ^{14}N, and ^{15}N.

One small molecule water analog is methanol, which is of interest because methanol changes the line shape or intensity of various OEC EPR signals.[21−25] ESEEM studies of the S_2-state multiline signal employing deuterated methanol (CD_3OH) show that methanol binds close to the OEC at a site with an effective $K_D \approx 80$ mM much lower than inhibitory concentrations (at 5 M MeOH there is a reversible impairment of O_2 evolution of only 14%).[26] The ESEEM was modeled as consistent with methanol bound to a proximal Ca^{2+},[27] although this was before the Mn_3Ca core geometry was known. We have recently used ENDOR and HYSCORE to probe the hyperfine coupling of ^{13}C-labeled methanol to the S_2-state of the OEC, and we interpret the observed weak ^{13}C hyperfine coupling to indicate that methanol does not bind directly to any of the Mn ions of the cluster.[28] The small coupling is consistent with ligation methanol to the Ca^{2+} of the OEC or in place of one of the nearby waters that hydrogen bond to bridging oxygens of the cluster.

Treatment with ammonia, however, appears more relevant to the task of identifying the substrate water. Ammonia is one of a set of amines that inhibits the OEC competitively with respect to Cl^-,[29,30] presumably at Cl^--sites identified in the X-ray structure.[2] Additionally, ammonia, alone among this set, inhibits at a second site that shows no competitiveness with Cl^-.[29,30] A detailed study of the effects of ammonia on S-state advancement showed minimal changes compared to untreated PSII, suggesting that the noncompetitive ammonia binding could be occurring at a structural site distinct from a substrate site.[31] More recently Navarro et al.[32] have shown that ammonia binding only modestly alters the water-derived substrate exchange kinetics as monitored with $^{16}O_2/^{16}O^{18}O/^{18}O_2$ isotope mass spectroscopy, and thus determination of the site of ammonia binding can in principle rule out a potential substrate site.[13,32]

Ammonia binding at the Cl^--independent site alters the line shape and ^{55}Mn hyperfine spacing of the S_2-state multiline EPR signal.[33] In the first pulse EPR study targeting the OEC, Britt and co-workers used ESEEM to show that ammonia binds directly to an Mn of the OEC poised in the S_2-state.[34] The EPR and ESEEM spectra of ammonia treated spinach "BBY" PSII preparations[35] advanced from the dark stable S_1-state to the S = 1/2 S_2-state via cryogenic illumination (195 K) were very similar to untreated PSII spectra, but upon annealing these samples briefly to 20 °C the subsequent EPR showed the S_2 multiline EPR signal is altered, and the corresponding ESEEM spectra revealed a new class of magnetically coupled nitrogen nuclei, with distinct features for $^{14}NH_3$ and $^{15}NH_3$-treated samples. The requirement of the annealing step to bind ammonia is consistent with the flash-induced luminescence studies of Velthuys[36] indicating ammonia binding at S_2 and S_3, but not at the S_1-state: the interpretation of the EPR results was

DOI: 10.1021/jacs.5b04768
J. Am. Chem. Soc. 2015, 137, 8829−8837

that upon cryogenic illumination the OEC can be oxidized by one electron to the S_2 electronic configuration, but the prior S_1-ligand set is frozen in place, and only upon annealing can ammonia bind to the Mn cluster, presumably replacing a water ligand.

Analysis of the ammonia ESEEM showed that the data were obtained close to the "exact cancellation" condition[37] where the magnitudes of internal hyperfine field and the external magnetic field are closely matched, leading to the appearance of three clear peaks, denoted ν_0, ν_-, and ν_+ in the spectrum. These peaks allow for the accurate determination of the nuclear quadrupole parameters for the $I = 1$ ^{14}N nucleus of the Mn-bound ammonia. The nuclear quadrupole interaction provides a point specific measure of the electronic wave function at the nucleus, measuring the magnitude of the electric field gradient (parametrized by e^2qQ) and its symmetry (the asymmetry parameter η ranges from 0 for pure axial symmetry to 1 for full rhombic symmetry).[38] In the exact cancellation limit ESEEM ^{14}N peaks appear close to the pure nuclear quadrupole resonance frequencies:

$$\nu_+ = \frac{1}{4}(3 + \eta)e^2qQ \quad \nu_- = \frac{1}{4}(3 - \eta)e^2qQ$$
$$\nu_0 = \frac{1}{2}\eta e^2qQ \tag{1}$$

For the OEC of spinach PSII, the measured quadrupolar parameters for the ^{14}N of bound ammonia were $e^2qQ = 1.61$ MHz and $\eta = 0.59$. This relatively high asymmetry parameter η is unusual for terminal NH_3 groups of C_{3v} symmetry, although it can be found in cases with strong asymmetric hydrogen bonding.[39,40] This led to the proposal that the ammonia-derived ligand could be bound in a lower symmetry form, specifically as a deprotonated amido (NH_2) bridge between two Mn ions of the OEC or between a Mn ion and the proximal Ca^{2+} ion.[34]

There are other lines of evidence in support of an ammonia-derived bridge. An S_2-minus-S_1 difference FTIR study of ammonia binding shows that ammonia treatment decreases the amplitude of a low-frequency mode assigned to an Mn−O−Mn vibration, suggesting that ammonia could replace a bridging oxygen such as O5.[41] Vinyard and Brudvig[13] have recently modeled the kinetics of ammonia-induced stabilization of the S_2-state, with the conclusion that the decrease in OEC reduction potential affected by ammonia is too large to be explained by a simple ammonia terminal ligation to a Mn(IV): they instead favor the ammonia derived ligand binding as a bridge in the S_2-state, with a μ-nitrido ligand replacing the O5 μ-oxo.[42] This view leaves open the proposed Mn(V)═O electrophile mechanism but would rule out the O5-centered radical coupling mechanism.

A counter view comes from the recent work of Navarro et al.[32] In addition to the oxygen isotope mass spectrometry, they used pulse EPR methods to probe the binding of magnetic ^{17}O-labeled water in competition with ammonia to explore the interplay of water and ammonia binding in the S_2-state. They concluded that ammonia binds at the W1 site on the dangler Mn, *trans* to the unique O5 bridge which they favor as a substrate in the radical coupling mechanism.[6,17] This is in direct contrast to the Vinyard and Brudvig[13] proposal that ammonia binds in place of the O5 bridge. As discussed, the specific substrate assignment gets at the heart of the current O−O bond forming mechanisms, so resolving this ammonia binding question is crucial.

In this work, we test the specific W1 site binding proposal of Navarro et al.[32] by employing pulse EPR spectroscopy to study ammonia binding in PSII from *Synechocystis*, contrasting wild-type with a D1-D61A mutant. The X-ray structure shows that aspartate D1-D61 hydrogen bonds to the dangler Mn water W1 (Figure 1A). In the mutant D1-D61A this aspartate is converted to the non-hydrogen-bonding residue alanine. The D1-D61A mutant gives rise to an altered S_2-state multiline EPR signal. The strong hyperfine coupling to nitrogen of D1His332 is maintained in the mutant, showing the unique Mn(III) of the S_2-state remains in the Mn1D position. Analysis of ^{15}N-labeled and natural abundance ^{14}N-ammonia treated samples shows that the ammonia hyperfine couplings are essentially the same between wild-type and D1-D61A, consistent with identical Mn(IV)-ligand binding sites. For the ^{14}N-ammonia sample, the magnitudes of the ^{14}N nuclear quadrupole coupling parameter e^2qQ also match between wild-type and D1-D61A. However, the nuclear quadrupole asymmetry parameter η is markedly different, with a relatively high rhombicity ($\eta = 0.42$) in the wild-type sample, consistent with a strong hydrogen bond to D1-D61A as shown in recent calculations,[43,44] compared to a very axial ($\eta = 0.04$) field gradient in the D1-D61A mutant lacking this specific hydrogen-bonding interaction to the W1 water ligand of Mn4A. This near-axial field gradient of the ^{14}N for ammonia bound to D1-D61A, characteristic of a terminal ammonia ligand, combined with the invariance of the maximum field gradient and hyperfine interaction, clearly points to terminal ammonia ligation at the Mn4A dangler Mn site, as previously proposed by Navarro et al.[32]

EXPERIMENTAL SECTION

Construction of *Synechocystis* Mutants and Propagation of Cultures. Construction of the D1-D61A mutation was described previously: the mutation was introduced into the *psbA-2* genes of *Synechocystis* sp. PCC 6803[45] and transformed into a host strain of *Synechocystis* that lacks all three *psbA* genes and contains a hexahistidine-tag (His-tag) fused to the C-terminus of CP47.[46] Single colonies were selected for their ability to grow on solid media containing 5 μg/mL kanamycin monosulfate. Solid media contained 5 mM glucose and 10 μM DCMU. The DCMU and antibiotic were omitted from the liquid cultures. The wild-type* (WT*) control strain was constructed in the same manner as the D1-D61A mutant, but with a transforming plasmid that bore no mutation. The designation "wild-type*" differentiates this strain from the native wild-type strain that contains all three psbA genes and is sensitive to antibiotics. Large-scale liquid cultures (each consisting of three 7-L cultures held in glass carboys) were propagated as described previously.[47] To verify the integrity of the mutant cultures that were harvested for the purification of PSII core complexes, an aliquot of each culture was set aside, and the sequence of the relevant portion of the *psbA-2* genes was obtained after PCR amplification of genomic DNA.[45] No traces of the wild-type codon was detected in any of the mutant cultures.

Purification of PSII Core Complexes. Oxygen-evolving PSII core complexes were purified as described previously in buffer A [1.2 M betaine, 10% (v/v) glycerol, 50 mM MES-NaOH (pH 6.0), 20 mM $CaCl_2$, 5 mM $MgCl_2$, 1 mM EDTA, and 0.03% (w/v) *n*-dodecyl β-D-maltoside] containing 50 mM histidine.[48] The purified PSII core complexes were concentrated to approximately 1 mg of Chl per mL, as described previously,[48] frozen as 0.5 mL aliquots in liquid N_2, and stored at −196 °C (vapor phase nitrogen).

Preparation of EPR Samples. Each sample (0.5 mg of Chl) was concentrated in a Centricon-100 centrifugal concentrator (Millipore Corporation, Bedford, MA) until only 60 μL remained. The concentrated sample was diluted with 1 mL of buffer A containing

DOI: 10.1021/jacs.5b04768
J. Am. Chem. Soc. 2015, 137, 8829−8837

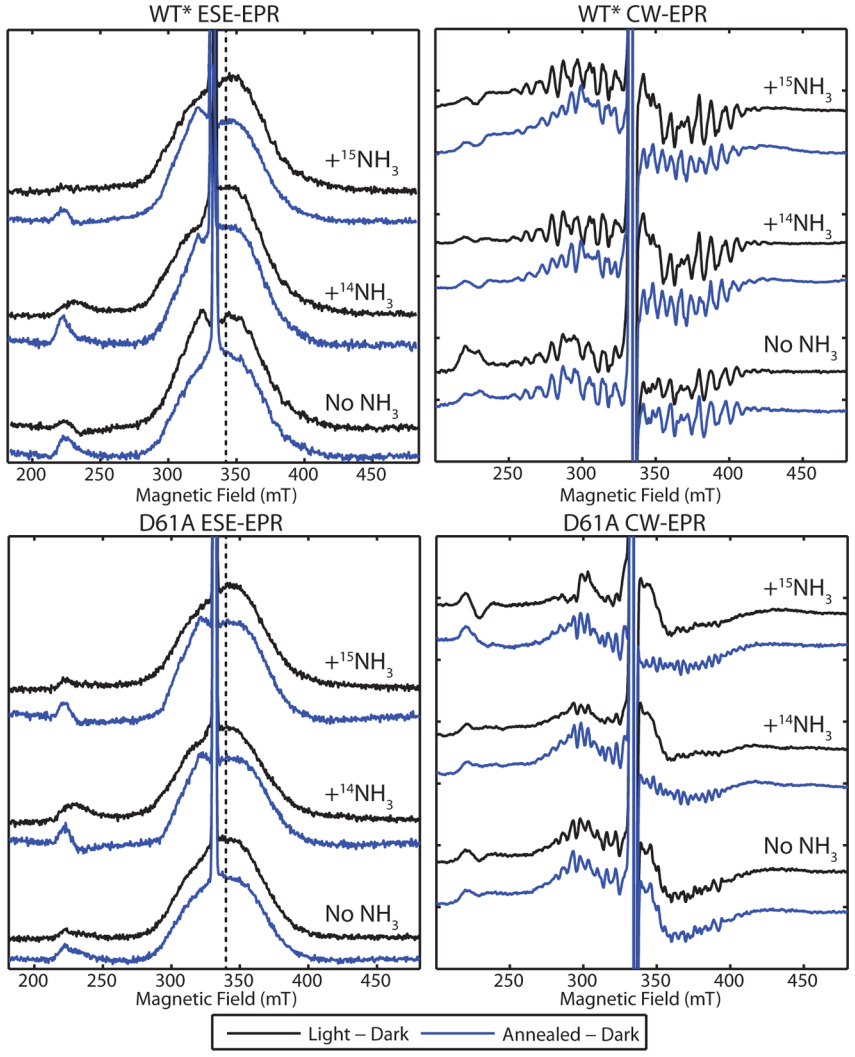

Figure 2. *X*-band pulse EPR difference spectra (left panels) and CW-EPR spectra right panels) of WT* (top panels) and the D1-D61A mutant (bottom panels). Black traces are the dark subtracted EPR spectra after illumination at 185 K, while blue traces are the dark subtracted spectra following annealing at 250 K. Acquisition parameters: ESE-EPR: microwave frequency = 9.329 GHz (WT*), 9.319 (D1-D61A); temperature = 4.5 K; $\pi/2$ MW = 12 ns; τ = 200 ns; rep. time =5 ms. CW-EPR: microwave frequency = 9.396 GHz; temperature = 7 K; MW power = 200 μW; mod. amp. = 5 G; conv. time = 82 ms. The vertical dashed line indicates the field positions for *X*-band ammonia ESEEM acquisition.

no buffering ions (i.e., no MES), and then reconcentrated until the volume was again 60 μL. The reconcentrated sample with then diluted with 1 mL of buffer A containing 50 mM HEPES-NaOH (pH 7.5) and 1 mM PPQB (added from a stock of 100 mM PPQB in DMSO). For NH_4Cl-treated samples, this pH 7.5 buffer also contained either $^{14}NH_4Cl$ or $^{15}NH_4Cl$ (99% ^{15}N enrichment, Cambridge Isotope Laboratories, Andover, MA) with a resulting free-base NH_3 concentration of 2 mM. The sample was again concentrated to 60 μL, then transferred to a 2.0 mM I.D., 2.4 mM O.D. quartz EPR tube under dim green light, dark-adapted for 30–45 min in total darkness on ice, and then frozen in liquid N_2.

To trap the S_2-state multiline signal prior to binding of ammonia, samples were illuminated for 4 min at 185 K using a liquid nitrogen-cooled gas-flow apparatus and a Sylvania ELH 300 W halogen-tungsten lamp (color temperature = 3350 K). This low-temperature illumination has been shown previously in both spinach PSII membrane preparations[31,34] and PSII cores from *Thermosynechococcus elongates*[32] to generate a "pre-bound" S_2-state which presents an EPR signal with no evidence off alteration by ammonia binding. Subsequently, these samples were annealed for 5 min at 250 K[31] to generate the ammonia-bound S_2-state with the ammonia-altered multiline EPR signal. In order to maximize the amount of ammonia-bound S_2-state, all samples were subsequently reilluminated at 200 K for 8 min, then again annealed 5 min at 250 K to ensure complete conversion to the ammonia-bound form.

CW EPR Spectroscopy. All continuous wave (CW) EPR spectra were collected at a temperature of 7 K using a Bruker ELEXSYS E500 *X*-band spectrometer equipped with an Oxford Instruments ESR900 cryostat and an ITC-503 temperature controller.

Pulse EPR and ENDOR. All pulse EPR and electron–nuclear double resonance (ENDOR) spectroscopic studies were performed at a temperature of 4.5 K using a Bruker ELEXSYS E580 pulse EPR spectrometer equipped with an Oxford-CF935 liquid helium cryostat and an ITC-503 temperature controller. *X*-band 3-pulse electron spin–echo envelope modulation (ESEEM) spectroscopy was performed with a Bruker MS-5 resonator using the pulse sequence: $\pi/2 - \tau - \pi 2 - T - \pi/2 -$ echo, with T the incremented time. Magnetic field swept pulse EPR spectra were acquired using the pulse sequence $\pi/2 - \tau - \pi -$ echo. *Q*-band Davies ENDOR was performed with the E580 EPR spectrometer equipped with a 250W RF amplifier (Amplifier Research) and an R.A. Isaacson-designed cylindrical TE_{011} resonator[49] adapted for pulse EPR use in an Oxford Instruments CF935 cryostat, and with the pulse sequence $\pi - t_{RF} - \pi_{RF} - t_{RF} - \pi/2 - \tau - \pi -$ echo, where π_{RF} is the optimized RF pulse length and t_{RF} is a fixed delay separating MW and RF pulses. Specific parameters for field positions, microwave frequencies, pulse, and delay lengths are

DOI: 10.1021/jacs.5b04768
J. Am. Chem. Soc. 2015, 137, 8829–8837

given in the captions of each figure. For PSII pulse EPR experiments, all spectra were acquired at a field position corresponding to $g = 1.98$, near the maximum of the S_2-state signal, yet not overlapping with the EPR spectrum of the persistent tyrosine radical $Y_D^{\bullet}$.

Pulse EPR Simulations. All pulsed EPR spectra were fit assuming an effective electron spin $S = 1/2$ ground state. Spectral simulations were performed using MATLAB 7.8.0 (R2009a) software package (The Mathworks Inc., Natick, MA) using the EasySpin 4.5.5 toolbox.[50,51]

RESULTS AND DISCUSSION

Pulse and CW EPR Signals. Figure 2 shows the pulse and CW *X*-band EPR spectra for WT* and D1-D61A PSII samples. The spectra for untreated, ^{15}N-ammonia treated, and natural abundance ammonia treated samples are displayed, and for each sample both illuminated-minus-dark and annealed-minus-dark difference spectra are shown. The *X*-band difference pulse spectra show near-Gaussian lineshapes resulting from the 1296 largely unresolved ^{55}Mn hyperfine transitions of the tetranuclear Mn complex with its four $I = 5/2$ ^{55}Mn nuclei.[5] The conventional field-modulated CW EPR spectra of the S_2-state show some resolved ^{55}Mn hyperfine lines (~19 lines for untreated PSII observed at *X*-band[52]). The *X*-band CW EPR signals for both untreated and ammonia treated WT* PSII samples are very similar to those observed for spinach PSII membrane preparations.[33,34] The D1-D61A mutant CW EPR spectra are further altered. In the absence of NH_3, it exhibits 20−22 resolved splittings of approximately 5.8 mT. In samples treated with NH_3, following advancement to the S_2-state and subsequent annealing, this spectrum is further altered, with 26−28 observed splittings of approximately 4.7 mT. In contrast to the WT* samples, the D61A mutant in the presence of NH_3 shows an altered ammonia multiline EPR signal before annealing at 250 K. This, combined with the observation of ^{14}N modulation in the *X*-band 3-pulse ESEEM of samples illuminated at 185 K that is identical to that of the annealed samples (see SI Figure S3), indicates that there may be a decrease in the energetic barrier to NH_3 binding to the S_2-state bypassing the requirement for the annealing step in WT* samples. A detailed EPR and ^{55}Mn ENDOR study of the untreated and ammonia treated D1-D61A samples is beyond the scope of this publication but is ongoing and will be published in a future paper.

His332 ESEEM. An ESEEM signal from the single histidine ligand to Mn, D1-H332 (Figure 1) was detected in the earliest *X*-band OEC ESEEM studies.[34,53,54] The ESEEM features were assigned to histidine via selective ^{15}N-histidine isotope labeling[55] and associated with D1-H332 via site-directed mutagenesis.[46] The resolution of these *X*-band (9 GHz) ESEEM features is relatively poor because the relatively low resonance fields (≈3400 G) are well below the exact cancellation limit that gives optimal ^{14}N ESEEM spectra. Tuning the nitrogen hyperfine selection via the choice of resonant microwave frequency is a useful tool for bioinorganic spectroscopy, including mixed valence Mn clusters such as the OEC and Mn catalase.[56] In the case of the S_2-state of the OEC, superior ESEEM resolution for the H332 nitrogen is obtained at the higher frequencies of the K_α and *Q* frequency bands (31−35 GHz).[57,58] In turn the *Q*-band ESEEM contribution from the more weakly coupled ammonia (see next section) is small, as shown in Figure S4. The high-resolution *Q*-band ESEEM of both WT* and D61 mutant are displayed in Figure 3, with time domain (top panels) and frequency domain

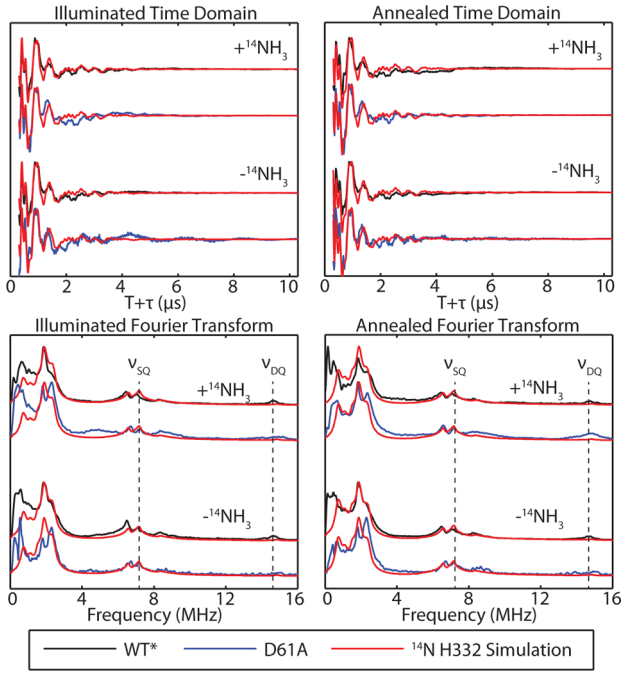

Figure 3. Comparison of *Q*-band 3-pulse ESEEM of WT* (black traces) and D1-D61A (blue traces) PSII samples treated with either natural abundance NH_3 (top traces in each panel) or no NH_3 (bottom traces in each panel). Left panels show the dark-subtracted ESEEM of the S_2-state after illumination for 4 min at 185 K, while the right panels show the dark subtracted ESEEM of the S_2-state after annealing for 5 min at 250 K. For each set, the top panel shows the time-domain data after subtraction of a biexponential decay function, and the bottom panel displays the Fourier transform of each time trace using cross-term averaging. Red traces represent the spectral simulation of the strongly coupled ^{14}N from His332 using the simulation parameters in Table 1. Acquisition parameters: microwave frequency = 33.920 GHz; magnetic field = 12240.5 mT; temperature = 4.5 K; $\pi/2$ MW pulse length = 12 ns; τ = 228 ns; T_{init} = 80 ns; rep. time = 5 ms.

(bottom panels) of untreated (illuminated-minus-dark) and ammonia-treated (annealed-minus-dark) samples. The ESEEM spectra for all cases are similar to the untreated WT* sample, with resolved low frequency transitions near the quadrupolar frequencies along with higher frequency single and double quantum nuclear spin transitions (marked by vertical dashed lines) from the $I = 1$ ^{14}N nucleus of the directly bound His322 nitrogen with an isotropic hyperfine coupling of ≈7 MHz which varies only slightly between the four S_2-state forms studied[58] (see Table 1). In PSII of wild-type *Synechocystis* this relatively large hyperfine coupling was taken as evidence that the His332-bonding Mn1D is the unique Mn(III) ion in the $Mn(IV)_3Mn(III)$-containing S_2-state,[58] an assignment consistent with multifrequency EPR and ENDOR studies of the OEC.[59]

Given the similar 3-pulse ESEEM of the ammonia-treated WT* sample to the untreated version, we can localize the Mn(III) to Mn1D in the ammonia-altered S_2-state form as well, as previously shown in PSII from *T. elongatus*.[32] The similar couplings measured for the D1-D61A mutant, both untreated and ammonia treated, demonstrate that this remains true for this specific OEC mutant. Therefore, at this key position opposite the dangler Mn, the electronic structure is invariant among all S_2-state forms studied here.

DOI: 10.1021/jacs.5b04768
J. Am. Chem. Soc. 2015, 137, 8829−8837

Table 1. ^{14}N HFI Simulation Parameters[a]

species	A_{iso} (MHz)	$A_{x,y,z}$ (MHz)	e^2Qq/h (MHz)	η	A and P Euler angles $(\alpha,\beta,\gamma)°$
^{14}N His 332					
WT*	7.21	[7.21 8.56 5.87]	1.973	0.801	(−16, 23, 6)
WT* + NH_3	7.23	[7.23 8.63 5.82]	1.960	0.830	(−21, 21, 14)
D61A	7.20	[7.21 8.57 5.79]	1.930	0.842	(−18, 24, 11)
D61A + NH_3		[7.21 8.57 5.80]	1.940	0.834	(−18, 24, 11)
^{14}N NH_3					
WT* + NH_3	2.33	[1.96 2.76 2.26]	1.616	0.402	(5, 98, 110)
Error[a]	±0.01	±[0.02 0.02 0.01]	±0.003	±0.008	±(1, 4, 7)
D61A + NH_3	2.36	[1.98 2.78 2.31]	1.536	0.042	(13, 51, 148)
Error[a]	±0.03	±[0.01 0.02 0.05]	±0.034	±0.001	±(1, 3, 3)

[a]Error was estimated using the standard deviations in the respective parameters obtained from least-squares fits of the three individual ESEEM traces collected with different τ values.

^{14}N-Ammonia ESEEM. At *Q*-band, the ESEEM is dominated by the strongly coupled H322 nitrogen. The ammonia nitrogen is much more weakly coupled and is best detected via ESEEM at the lower *X*-band microwave frequency[32,34] (*vide infra*). Figure 4 displays the 3-pulse annealed-minus-dark ESEEM of the natural abundance (99.5% ^{14}N) ammonia samples for both WT* and the D1-D61A mutant. Time domain spectra for three different τ values are shown in the top panels, and the corresponding Fourier transform spectra are displayed in the bottom panels, with experimental spectra shown in black and simulations in red. The 3-pulse time domain spectra are deeply modulated and resemble prior results in PSII from spinach[34] and from *T. elongatus*.[32] These deep modulations are absent in 3-pulse ESEEM spectra obtained with ^{15}N-ammonia (Figure S1), therefore they can be directly assigned to ^{14}N of ammonia.

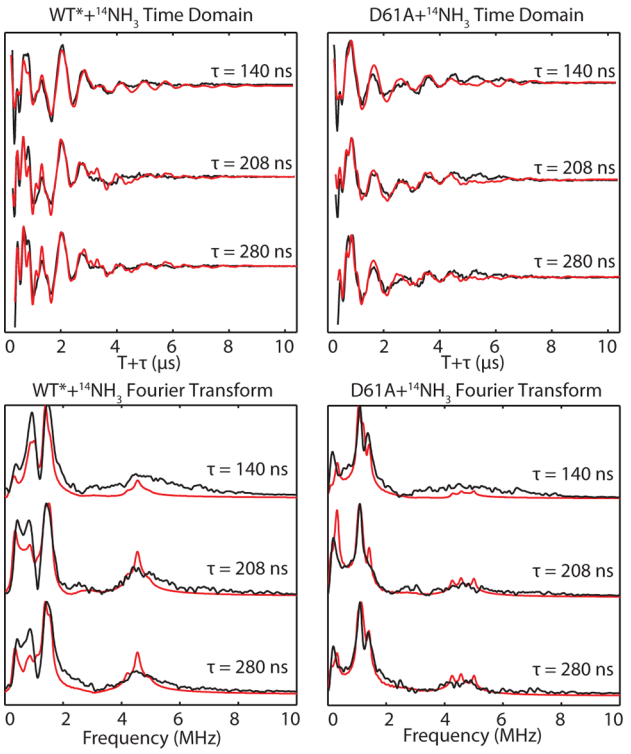

Figure 4. *X*-band 3-pulse ESEEM of the natural abundance ^{14}N-ammonia-bound S_2-state in WT* (left-hand panels) and the D1-D61A mutant (right-hand panels). For each, the top panel shows the time-domain data after subtraction of a biexponential decay function, and the bottom panel displays the Fourier transform of each time trace using cross-term averaging. Black traces represent the experimental data, while red traces represent the simulated spectrum using the simulation parameters in Table 1. Acquisition parameters: microwave frequency = 9.329 GHz (WT*), 9.319 (D1-D61A); magnetic field = 336.4 mT (WT*), 335.5 mT (D1-D61A); temperature = 4.5 K; $\pi/2$ MW pulse length = 12 ns; T_{init} = 80 ns; rep. time = 5 ms.

The Fourier transform spectra of the WT* sample show three low-frequency transitions (<2 MHz) that correspond closely to the three NQR transitions ν_0, ν_-, and ν_+ for the spin I = 1 ^{14}N nucleus. The simulations for the ESEEM at the three different τ values properly track the intensity of these three transitions. The simulations (in red) include nuclear quadrupole parameters of e^2qQ = 1.61 MHz and η = 0.40 (Table 1). These are the average values obtained for each of the three τ values, where each τ set was first independently evaluated, giving the reported error range for e^2qQ and η. This e^2qQ value is identical to the value (1.61 MHz) we determined in spinach BBY PSII membranes.[34] The asymmetry parameter is somewhat higher in the spinach PSII preparation (η = 0.59). The values determined in the recent *T. elongatus* study are similar, e^2qQ = 1.52 MHz and η = 0.47.[32]

A fourth ^{14}N ESEEM transition appears at a higher frequency, ≈4.5 MHz. We assign this to the ^{14}N double quantum transition, ν_{dq}, and its specific frequency encodes information about the hyperfine coupling as well as the nuclear quadrupole coupling.[34,37] The simulation provides ^{14}N hyperfine matrix components of $\tilde{A}$ = [1.961, 2.763, 2.262 MHz] corresponding to an isotropic hyperfine coupling A_{iso} = 2.32 MHz. Scaling the tensor components by the ratio of magnetogyric ratios for ^{15}N and ^{14}N ($\gamma(^{15}N)/\gamma(^{14}N)$ = 1.40) gives ^{15}N ENDOR simulations that approximately match experimental Davies pulse ENDOR of the annealed ^{15}N-ammonia sample (Figure S2). The WT* *Synechocystis* ^{14}N-ammonia hyperfine coupling also is very close to the values of $^{14}NA_{iso}$ = 2.29 MHz determined in the prior spinach study and 2.36 MHz in the *T. elongatus* study[32] (Table 2) .

The ESEEM spectra of the D1-D61A mutant are quite different from those of WT*. This is evident in the time domain, as the modulation is dominated by a single component with a period of approximately 1030 ns. The Fourier transform spectrum shows that ν_- and ν_+ for the D1-D61A sample are close in frequency, nearly merged into a single peak that gives rise to the 1030 ns period modulation, and ν_0 has moved to much lower frequency, indicating a much smaller asymmetry parameter η. The parameters for the displayed simulation are $\tilde{A}$ = [1.984, 2.775, 2.311 MHz], A_{iso} = 2.36 MHz, e^2qQ = 1.54

DOI: 10.1021/jacs.5b04768
J. Am. Chem. Soc. 2015, 137, 8829−8837

Table 2. Comparison of $^{14}NH_3$ HFI and NQI Parameters

species	A_{iso} (MHz)	$A_{x,y,z}$ (MHz)	e^2Qq/h (MHz)	η	A and P Euler angles $(\alpha,\beta,\gamma)°$	ref
Synechocystis						
WT* + NH_3	2.33	[1.96 2.76 2.26]	1.616	0.402	(−5, 98, 110)	This work
D61A + NH_3	2.36	[1.98 2.78 2.31]	1.536	0.042	(13, 51, 148)	This work
T. elongatus						
WT* + NH_3	2.36	[2.77 2.62 1.69]	1.52	0.47	Not reported	31
Spinach						
WT* + NH_3	2.29	[2.09 2.09 2.69]	1.61	0.59	(0, 0, 0)	33

MHz, and η = 0.042 (Table 1). Comparing WT* and D1-D61A ESEEM results, the near equivalence of the hyperfine couplings (A) and the strength of the field gradient (e^2qQ) indicate that ammonia is binding in D1-D61A mutant at the same site as the WT* PSII. The collapse by a factor of 10 in the η value, from 0.40 to 0.042, indicates that without the hydrogen bond from the D1-D61 aspartate side chain (Figure 1) the bound ammonia-derived ligand has an axialy symmetric field gradient characteristic of a terminal ammonia ligand. This provides very strong evidence that the ammonia binding site in the S_2-state corresponds to the crystallographically defined W1 water site in the Mn4A dangler Mn.[32,43]

Discussion. High-resolution X-ray crystal structures of PSII show the carboxylate side chain of D1-Asp61 participating in a hydrogen bond to the W1 water ligand of the dangling Mn (Mn4A) of the OEC (Figure 1A). It has previously been observed that certain mutations of this aspartate residue, including the D1-D61A used here, drastically slow O_2 release.[60] This reduction in activity perhaps results from disruption of a proton egress pathway that the X-ray structures reveal has D1-D61 at its beginning. Indeed, replacement of the carboxylate anion side chain with a neutral carboxamide (D61N) slows O_2 release (up to 50 ms) in a pH-dependent manner.[61] Difference FTIR results indicate that the Asp-to-Ala mutation removes the hydrogen bond to W1 and that this may cause the reduction of O_2-evolution efficiency in this mutant.[48]

As shown in Figure 2, the D1-D61A mutant gives rise to a light-induced S_2-state EPR signal that is qualitatively similar to other S = 1/2 S_2-state multiline signal forms, with a nearly Gaussian line shape plus some small line shape contribution from a modest amount of g-anisotropy. Some ^{55}Mn hyperfine features are resolved in the field-modulated CW EPR spectrum for both WT* and D61A mutant. However, the spacing between the ^{55}Mn hyperfine splittings is changed for the mutant and more resonances are apparent. A similar, so-called "altered multiline" signal is observed for the D1-H332E mutant and for calcium-depleted and strontium-substituted PSII preparations. An altered multiline signal is also the hallmark for the ammonia-treated PSII that we investigated earlier[34] and in the current study. Advanced EPR studies centered around ^{55}Mn ENDOR have shown that, in the cases of Sr-substitution, NH_3-binding,[44] and Ca-depletion,[62] this altered multiline CW EPR signal results from relatively modest changes in the degree of ^{55}Mn hyperfine anisotropy due to slight changes in the Mn(III) fine structure parameter, but overall the electronic structure of the OEC is preserved.

Evidence for this preservation in the D61A mutant is found in the Q-band ESEEM data which show very similar hyperfine couplings to the strongly coupled ^{14}N of D1-His332 for both WT* and D1-D61A (Figure 3). Specifically, this means that the single Mn(III) ion at the S_2-state is localized at the Mn1D position, the bonding partner to His332. We also observe that the locality of the Mn(III) ion is unchanged in both systems upon addition of ammonia.

Interestingly, the X-band ESEEM shows much more dramatic differences between the ammonia-treated WT* and the D1-D61A PSII (Figure 4). These spectral features are assigned to the ^{14}N nucleus of the ammonia ligand, with our analysis indicating that the hyperfine coupling to the ammonia nitrogen in the ammonia-altered S_2-state signal is very close to that of the WT* PSII, and consistent with ligation to an Mn(IV) ion.[32] The low-frequency portion of the Fourier transformed ESEEM spectra indicates that the origin of the dramatic spectral differences is owed to a large decrease in the electric field gradient asymmetry in the D1-D61A mutant, in which D1-D61 is not present to provide a hydrogen bond to the ammonia. This behavior was predicted in computational models of the OEC that had ammonia binding as a terminal ligand at the Mn4A W1 binding site.[43,44] Thus, these results provide conclusive and direct proof of this binding model for ammonia at the S_2-state of the OEC.

Since the bridging oxo O5 is not the site where ammonia binds, the Siegbahn radical coupling mechanism for O−O bond formation remains viable.[6,17] At the same time, we do not consider this result to rule out the alternative electrophile/nucleophile model for O−O bond formation, since from the X-ray structures the dangler Mn4A W2 water is better positioned to interact with the Ca^{2+}-bound W3 than that of the W1 water, which is shown to be displaced by ammonia.

The substrate isotope exchange kinetics are modestly altered by ammonia binding,[32] which could be consistent with ammonia replacing water at a site *cis* to the W2 water site on the dangler Mn4A. While W1 does not appear to represent a substrate site directly involved in O−O bond formation, it may represent a "holding site" for subsequent substrate water so that new substrate waters are allowed to bind rapidly following elimination of O_2. The atomic-level mechanism of how ammonia inhibits PSII-catalyzed water oxidation is still unclear. However, we show here that this process begins with ammonia binding terminally to the dangling manganese of the OEC, most likely at the S_2-state. Ammonia cannot bind earlier in the Kok cycle, as the Mn4A site is in the Mn(III) oxidation state in S_0 and S_1-states, placing an electron in the σ-antibonding $3d_{z^2}$ orbital. Upon oxidation of this dangler Mn4A to Mn(IV) in the $S_1 \rightarrow S_2$ transition, a recent computational study has concluded that the W2 water is deprotonated to a hydroxide,[63] which would make it easier for ammonia to preferentially displace the remaining W1 water. The influence the bound ammonia has on the electronic structures of higher S-states is unknown, but the recent advanced EPR characterization of the S_3-state[6] presents an exciting new target for such studies.

DOI: 10.1021/jacs.5b04768
J. Am. Chem. Soc. 2015, 137, 8829−8837

■ ASSOCIATED CONTENT

Supporting Information

ESEEM and ENDOR of PSII samples treated with ^{15}N-ammonia; comparison of ESEEM for illuminated and annealed ammonia treated PSII; analysis of the small contribution of ammonia to the *Q*-band ESEEM. The Supporting Information is available free of charge on the ACS Publications website at DOI: 10.1021/jacs.5b04768.

■ AUTHOR INFORMATION

Corresponding Author

*rdbritt@ucdavis.edu

Notes

The authors declare no competing financial interest.

■ ACKNOWLEDGMENTS

This work was funded by the Division of Chemical Sciences, Geosciences, and Biosciences (R.D.B. grant DE-FG02-11ER16282 for EPR spectroscopy; and R.J.D. grant DE-SC0005291 for mutant construction and sample preparation) of the Office of Basic Energy Sciences of the U.S. Department of Energy.

■ REFERENCES

(1) Kok, B.; Forbush, B.; McGloin, M. *Photochem. Photobiol.* **1970**, *11*, 457−475.
(2) Umena, Y.; Kawakami, K.; Shen, J. R.; Kamiya, N. *Nature* **2011**, *473*, 55−60.
(3) Suga, M.; Akita, F.; Hirata, K.; Ueno, G.; Murakami, H.; Nakajima, Y.; Shimizu, T.; Yamashita, K.; Yamamoto, M.; Ago, H.; Shen, J.-R. *Nature* **2015**, *517*, 99−103.
(4) Ferreira, K. N.; Iverson, T. M.; Maghlaoui, K.; Barber, J.; Iwata, S. *Science* **2004**, *303*, 1831−1838.
(5) Peloquin, J. M.; Campbell, K. A.; Randall, D. W.; Evanchik, M. A.; Pecoraro, V. L.; Armstrong, W. H.; Britt, R. D. *J. Am. Chem. Soc.* **2000**, *122*, 10926−10942.
(6) Cox, N.; Retegan, M.; Neese, F.; Pantazis, D. A.; Boussac, A.; Lubitz, W. *Science* **2014**, *345*, 804−808.
(7) Hoganson, C. W.; Babcock, G. T. *Science* **1997**, *277*, 1953−1956.
(8) Britt, R. D.; Oyala, P. H. *Science* **2014**, *345*, 736−736.
(9) Cotruvo, J. A.; Stich, T. A.; Britt, R. D.; Stubbe, J. *J. Am. Chem. Soc.* **2013**, *135*, 4027−4039.
(10) Pecoraro, V. L.; Baldwin, M. J.; Caudle, M. T.; Hsieh, W. Y.; Law, N. A. *Pure Appl. Chem.* **1998**, *70*, 925−929.
(11) Limburg, J.; Szalai, V. A.; Brudvig, G. W. *J. Chem. Soc., Dalton Trans.* **1999**, 1353−1361.
(12) Vrettos, J. S.; Limburg, J.; Brudvig, G. W. *Biochim. Biophys. Acta* **2001**, *1503*, 229−245.
(13) Vinyard, D. J.; Brudvig, G. W. *Biochemistry* **2015**, *54*, 622−628.
(14) Taguchi, T.; Gupta, R.; Lassalle-Kaiser, B.; Boyce, D. W.; Yachandra, V. K.; Tolman, W. B.; Yano, J.; Hendrich, M. P.; Borovik, A. S. *J. Am. Chem. Soc.* **2012**, *134*, 1996−1999.
(15) Gupta, R.; Taguchi, T.; Lassalle-Kaiser, B.; Bominaar, E. L.; Yano, J.; Hendrich, M. P.; Borovik, A. S. *Proc. Natl. Acad. Sci. U.S.A.* **2015**, *112*, 5319−5324.
(16) Britt, R. D.; Suess, D. L. M.; Stich, T. A. *Proc. Natl. Acad. Sci. U.S.A.* **2015**, *112*, 5265−5266.
(17) Siegbahn, P. E. M. *Biochim. Biophys. Acta* **2013**, *1827*, 1003−1019.
(18) Pantazis, D. A.; Ames, W.; Cox, N.; Lubitz, W.; Neese, F. *Angew. Chem., Int. Ed.* **2012**, *51*, 9935−9940.
(19) Tagore, R.; Chen, H.; Crabtree, R. H.; Brudvig, G. W. *J. Am. Chem. Soc.* **2006**, *128*, 9457−9465.
(20) Siegbahn, P. E. M. *J. Am. Chem. Soc.* **2013**, *135*, 9442−9449.
(21) Zimmermann, J. L.; Rutherford, A. W. *Biochemistry* **1986**, *25*, 4609−4615.
(22) Messinger, J.; Nugent, J. H. A.; Evans, M. C. W. *Biochemistry* **1997**, *36*, 11055−11060.
(23) Deak, Z.; Peterson, S.; Geijer, P.; Ahrling, K. A.; Styring, S. *Biochim. Biophys. Acta* **1999**, *1412*, 240−249.
(24) Noering, B.; Shevela, D.; Renger, G.; Messinger, J. *Photosynth. Res.* **2008**, *98*, 251−260.
(25) Su, J.-H.; Cox, N.; Ames, W.; Pantazis, D. A.; Rapatskiy, L.; Lohmiller, T.; Kulik, L. V.; Dorlet, P.; Rutherford, A. W.; Neese, F.; Boussac, A.; Lubitz, W.; Messinger, J. *Biochim. Biophys. Acta* **2011**, *1807*, 829−840.
(26) Force, D. A.; Randall, D. W.; Lorigan, G. A.; Clemens, K. L.; Britt, R. D. *J. Am. Chem. Soc.* **1998**, *120*, 13321−13333.
(27) Britt, R. D.; Campbell, K. A.; Peloquin, J. M.; Gilchrist, M. L.; Aznar, C. P.; Dicus, M. M.; Robblee, J.; Messinger, J. *Biochim. Biophys. Acta* **2004**, *1655*, 158−171.
(28) Oyala, P. H.; Stich, T. A.; Stull, J. A.; Yu, F.; Pecoraro, V. L.; Britt, R. D. *Biochemistry* **2014**, *53*, 7914−7928.
(29) Sandusky, P. O.; Yocum, C. F. *Biochim. Biophys. Acta* **1984**, *766*, 603−611.
(30) Sandusky, P. O.; Yocum, C. F. *Biochim. Biophys. Acta* **1986**, *849*, 85−93.
(31) Boussac, A.; Rutherford, A. W.; Styring, S. *Biochemistry* **1990**, *29*, 24−32.
(32) Navarro, M. P.; Ames, W. M.; Nilsson, H.; Lohmiller, T.; Pantazis, D. A.; Rapatskiy, L.; Nowaczyk, M. M.; Neese, F.; Boussac, A.; Messinger, J.; Lubitz, W.; Cox, N. *Proc. Natl. Acad. Sci. U.S.A.* **2013**, *110*, 15561−15566.
(33) Beck, W. F.; Depaula, J. C.; Brudvig, G. W. *J. Am. Chem. Soc.* **1986**, *108*, 4018−4022.
(34) Britt, R. D.; Zimmermann, J. L.; Sauer, K.; Klein, M. P. *J. Am. Chem. Soc.* **1989**, *111*, 3522−3532.
(35) Berthold, D. A.; Babcock, G. T.; Yocum, C. F. *FEBS Lett.* **1981**, *134*, 231−234.
(36) Velthuys, B. R. *Biochim. Biophys. Acta* **1975**, *396*, 392−401.
(37) Flanagan, H. L.; Singel, D. J. *J. Chem. Phys.* **1987**, *87*, 5606−5616.
(38) Das, T. P.; Hahn, E. L. *Nuclear quadrupole resonance spectroscopy*; Academic Press: New York, 1958; pp223.
(39) Edmonds, D. T.; Hunt, M. J.; Mackay, A. L. *J. Magn. Reson.* **1973**, *9*, 66−74.
(40) Edmonds, D. T.; Summers, C. P. *J. Magn. Reson.* **1973**, *12*, 134−142.
(41) Hou, L.-H.; Wu, C.-M.; Huang, H.-H.; Chu, H.-A. *Biochemistry* **2011**, *50*, 9248−9254.
(42) Pokhrel, R.; Brudvig, G. W. *Phys. Chem. Chem. Phys.* **2014**, *16*, 11812−11821.
(43) Schraut, J.; Kaupp, M. *Chem.—Eur. J.* **2014**, *20*, 7300−7308.
(44) Lohmiller, T.; Krewald, V.; Navarro, M. P.; Retegan, M.; Rapatskiy, L.; Nowaczyk, M. M.; Boussac, A.; Neese, F.; Lubitz, W.; Pantazis, D. A.; Cox, N. *Phys. Chem. Chem. Phys.* **2014**, *16*, 11877−11892.
(45) Chu, H. A.; Nguyen, A. P.; Debus, R. J. *Biochemistry* **1994**, *33*, 6137−6149.
(46) Debus, R. J.; Campbell, K. A.; Gregor, W.; Li, Z. L.; Burnap, R. L.; Britt, R. D. *Biochemistry* **2001**, *40*, 3690−3699.
(47) Strickler, M. A.; Walker, L. M.; Hillier, W.; Britt, R. D.; Debus, R. J. *Biochemistry* **2007**, *46*, 3151−3160.
(48) Debus, R. J. *Biochemistry* **2014**, *53*, 2941−2955.
(49) Flores, M.; Isaacson, R. A.; Calvo, R.; Feher, G.; Lubitz, W. *Chem. Phys.* **2003**, *294*, 401−413.
(50) Stoll, S.; Schweiger, A. *J. Magn. Reson.* **2006**, *178*, 42−55.
(51) Stoll, S.; Britt, R. D. *Phys. Chem. Chem. Phys.* **2009**, *11*, 6614−6625.
(52) Dismukes, G. C.; Siderer, Y. *Proc. Natl. Acad. Sci. U.S.A.* **1981**, *78*, 274−278.
(53) DeRose, V. J.; Yachandra, V. K.; McDermott, A. E.; Britt, R. D.; Sauer, K.; Klein, M. P. *Biochemistry* **1991**, *30*, 1335−1341.
(54) Zimmermann, J. L.; Boussac, A.; Rutherford, A. W. *Biochemistry* **1993**, *32*, 4831−4841.

DOI: 10.1021/jacs.5b04768
J. Am. Chem. Soc. 2015, 137, 8829−8837

(55) Tang, X. S.; Diner, B. A.; Larsen, B. S.; Gilchrist, M. L.; Lorigan, G. A.; Britt, R. D. *Proc. Natl. Acad. Sci. U.S.A.* **1994**, *91*, 704−708.
(56) Stich, T. A.; Whittaker, J. W.; Britt, R. D. *J. Phys. Chem. B* **2010**, *114*, 14178−14188.
(57) Yeagle, G. J.; Gilchrist, M. L.; McCarrick, R. M.; Britt, R. D. *Inorg. Chem.* **2008**, *47*, 1803−1814.
(58) Stich, T. A.; Yeagle, G. J.; Service, R. J.; Debus, R. J.; Britt, R. D. *Biochemistry* **2011**, *50*, 7390−7404.
(59) Cox, N.; Rapatskiy, L.; Su, J.-H.; Pantazis, D. A.; Sugiura, M.; Kulik, L.; Dorlet, P.; Rutherford, A. W.; Neese, F.; Boussac, A.; Lubitz, W.; Messinger, J. *J. Am. Chem. Soc.* **2011**, *133*, 3635−3648.
(60) Hundelt, M.; Hays, A. M. A.; Debus, R. J.; Junge, W. *Biochemistry* **1998**, *37*, 14450−14456.
(61) Dilbeck, P. L.; Hwang, H. J.; Zaharieva, I.; Gerencser, L.; Dau, H.; Burnap, R. L. *Biochemistry* **2012**, *51*, 1079−1091.
(62) Lohmiller, T.; Cox, N.; Su, J.-H.; Messinger, J.; Lubitz, W. *J. Biol. Chem.* **2012**, *287*, 24721−24733.
(63) Ames, W.; Pantazis, D. A.; Krewald, V.; Cox, N.; Messinger, J.; Lubitz, W.; Neese, F. *J. Am. Chem. Soc.* **2011**, *133*, 19743−19757.

DOI: 10.1021/jacs.5b04768
J. Am. Chem. Soc. 2015, 137, 8829−8837